Journal of Materials Chemistry A

Accepted Manuscript

ROYAL SOCIETY OF CHEMISTRY

www.rsc.org/materialsA

Vertically Oriented Few-layer Graphene-Nanocup Hybrid Structured Electrodes for High-performance Supercapacitor

Jun Lei Qi, Xu Wang, Jing Huang Lin, Fu Zhang, Ji Cai Feng* and Wei-Dong Fei*

State Key Laboratory of Advanced Welding and Joining, Harbin Institute of Technology, Harbin 150001, China

*Corresponding authors: Tel. /fax: 86-451-86418146;

E-mail: fengjc@hit.edu.cn (J C Feng) and wdfei@hit.edu.cn(W-D Fei) ;

Abstract:

A high-performance supercapacitor was successfully developed using graphene-based 3D hybrid nanostructured electrodes. The 3D hybrid nanostructure, consisting of vertically oriented few-layer graphene (VFG) grown on alveolate Pt film with high-density nanocups, was synthesized by a simple and efficient "*one-step*" method. The 3D VFG-nanocup hybrid structured electrodes showed a high specific surface for ion transmission and storage, which contributes to the enhancement of areal capacitance by accommodating more charges in a given footprint area than that of conventional plane-structured electrodes. Electrochemistry results indicate that the 3D VFG-nanocup hybrid structured electrodes exhibit high specific capacitance up to 1052 μF/cm^2 (triple that of VFG-plane, at approximately 337 μF/cm^2), and a good cycling stability with about 93% capacitance retention after 3000 cycles. These easily fabricated, high-performance 3D hybrid nanostructured electrodes offer great promise in energy storage device applications.

Keywords:

Vertically oriented few-layer graphene, nanocups structure, supercapacitor, high surface area

1. Introduction

Electrical double-layer capacitors (EDLCs) exhibit huge potential for efficient energy storage applications because of their high specific power capability, fast charge/discharge processes, and long cycle life.[1-5] Because they possess higher power densities compared with conventional batteries and several orders of magnitude higher capacitances than dielectric capacitors, EDLCs can function as temporary energy storage devices for power applications in the electronics industry.[1-4] However, the energy density of EDLCs is relatively low, which restricts their further application.[3] According to the energy storage mechanism of EDLC, in which the energy is stored in the form of electrostatic charge accumulation at the electrode-electrolyte interface,[1, 4] the performance of EDLCs essentially depends on the specific surface area of the electrode. Therefore, increasing the specific surface area is desired to achieve enhanced capacitance and thus improve the energy density. Along this line, several carbon nanomaterials with large surface areas such as nanoporous carbon, activated carbon, carbon nanofibers, carbon nanotubes (CNTs), reduced multilayer graphene oxide (RMGO), and one- to few-layer graphene have been explored as electrode materials.[5-10] Recently, several studies have indicated that electrode materials with 3D structures show markedly improved capacitance. This unique structure favors ion diffusion and storage because of its inherent non-stacking morphology, which can provide a large specific surface area. Miller *et al.*[3] successfully fabricated vertically oriented few-layer graphene (VFG) electrodes on Ni substrates using plasma-enhanced chemical vapor deposition (PECVD); these electrodes showed a large improvement in capacitance. Ajayan *et al.*[10] and Lee et *al.*[11] reported that remarkably higher capacitance could be obtained than conventional stacked RMGO-based capacitors with the utilization of vertical alignment and the

open architecture of RMGO in electrodes. To further increase capacitance, more complicated hybrid construction of electrodes has been proposed.[12, 13] Ajayan *et al.*[13] reported 3D hybrid nanostructured electrodes consisting of vertically aligned CNTs on highly porous carbon nanocups. The 3D hybrid nanostructured electrodes showed highly improved specific surface area and areal capacitance compared with pure CNT-based electrodes.[13]

To achieve higher areal capacitance more effectively, here we report a simple and efficient method to fabricate 3D VFG-nanocup hybrid structured electrodes using VFG grown in situ on alveolate Pt film with high-density nanocups. The structural and electrochemical characterization of the 3D electrodes indicates greatly enhanced performance over an electrode purely based on a planar substrate.

2. Experimental

We constructed the 3D VFG-nanocup hybrid structured electrodes by *one-step* PECVD. Fig. 1 shows a detailed schematic of the fabrication process. Annealing was performed for the Pt film first. A Pt film with a thickness of about 200 nm was deposited using direct-current magnetron sputtering onto a Si (100) substrate. The as-deposited Pt film was placed in the chamber of a PECVD system, and the chamber was pumped down to 5 Pa. Then, the Pt film was treated at 800 ^{o}C for 60 min in an Ar gas atmosphere (the Ar gas flow was kept at 20 sccm) under a pressure of 200 Pa. This process can induce a morphology transformation of Pt film from a smooth to a porous surface with high-density nanocups, as shown in Fig. 1. Subsequently, VFG were grown in situ on the surface of Pt nanocups by radio frequency PECVD in a mixture of CH_4 and Ar with a constant flow ratio of 5/95 (the total gas flow was kept at 100 sccm) for 30 min. The total gas pressure was fixed at 600 Pa, and the radio frequency power was 200 W. The obtained samples (VFG-nanocups) were assembled

into simple EDLCs consisting of two VFG-nanocup electrodes, a polypropylene film separator, and aqueous electrolyte solution in a layered structure. For comparison, samples of VFG grown on 800-nm-thick Pt film were prepared under the same conditions in advance.

The morphology and structure of the obtained samples were characterized by scanning electron microscopy (SEM; JEOL JSM-6700F), transmission electron microscopy (TEM) and high-resolution TEM (HRTEM; JEOL TEM-2010 operated at 200 kV), and Raman spectroscopy (Renishaw-InVia with an excitation wavelength of 532 nm).

Cyclic voltammetry (CV), galvanostatic charge/discharge (CD), and self-discharge testing were conducted in a three-electrode system containing an aqueous electrolyte solution of 6 M KOH within the potential window from -0.2 to 0.4 V *vs*. a saturated calomel electrode. The obtained samples were cut into 1 cm×1 cm pieces and attached to the electrode holder, acting as working electrodes. A 2 cm×1 cm piece of Pt film was used as an auxiliary electrode, and a calomel electrode was used as a reference electrode. These tests were conducted using an electrochemical workstation (CHI-760E). Complex-plane electrochemical impedance spectrum (EIS) testing was carried out in the same three-electrode system using an electrochemical workstation (PARSTAT 2273). EIS testing was performed at a DC bias of 0 V over a frequency range of 100 kHz to 100 MHz.

EDLCs based on VFG-nanocup hybrid structured electrodes were assembled in a symmetric two-electrode system with a layered structure between two pieces of plastic sheet.[14, 15] Two pieces of 1 cm×1 cm VFG-nanocup samples separated by a porous polypropylene film were used as two electrodes in 6 M KOH aqueous electrolyte solution. The aqueous electrolyte solution was for ionic transmission while

preventing electronic current from discharging the cell.[16] A Pt wire was clipped onto the end of each current collector.

3. Results and Discussion

Fig. 2a-d show schematic drawings of SEM images corresponding to the 3D VFG-nanocup hybrid structured electrodes. As shown in Fig. 2a and b, large amounts of alveolate nanocups with an average diameter of approximately 800 nm were uniformly formed on the Pt film (200 nm thick) after annealing (at 800 ^{o}C for 60 min). This behavior is mostly due to the size-induced melting point depression in nanometer-sized thickness film, which leads to surface melting on Pt thin film at relatively low temperatures.[17, 18] Aggregation of the native grains into the clusters occurred in the quasi-liquid Pt film caused by surface energy minimization upon thermal annealing,[19-21] which facilitates the formation of this nanocup morphology. Obviously, this highly porous nanocup structure provides a larger surface area for graphene growth than a planar substrate. Moreover, the obtained VFG are uniformly and densely distributed on the surface of Pt nanocups, as shown in Fig. 2c. In the high-magnification SEM image (Fig. 2d), it is clear that both the bottom and side wall of the nanocups are covered with VFG. The inset of Fig. 2c shows the side-view SEM image of the VFG-nanocup. The VFG nanosheets vertically grow from the surface of the Pt nanocup with densely exposed bending edge planes and random expansive open areas. The height of the VFG nanosheets can be obtained from the cross-sectional view of VFG in side-view SEM and TEM images (The inset of Fig. 2c and Fig. 2e) accurately. The complete VFG nanosheets were separated from the substrate by mechanical exfoliation and the average net height of VFG nanosheets is estimated to be around 100 nm. As shown in Fig 2f, the thickness of the VFG edge varies between 3 and 6 graphene layers, with an interplanar spacing of 0.34 nm,

which suggests that the as-grown VFG is few-layer graphene.

It is known that the surface melting and eventual agglomeration in metal films at high temperature are thickness-dependent.[17, 18] Consequently, thicker Pt films (800 nm) were used for VFG growth to prevent the formation of agglomeration on the Pt film surface upon thermal annealing (at 800 ^{o}C). The SEM, TEM, and HRTEM images of VFG grown on the thick Pt film (VFG-plane) are presented in Fig. 3. As shown in Fig. 3a, the thicker Pt film retains a very smooth and planar surface, with well-organized, mutually connected VFG uniformly distributed on it. This is mostly due to the attenuation of size-induced melting with increasing film thickness. Furthermore, the morphology of the obtained VFG remains approximately the same as that grown on Pt nanocups, which are vertically standing on the surface of the Pt film, as shown in Fig. 3b. Fig. 3c shows a typical TEM image of VFG, where all graphene flakes are connected to each other at the roots. The average height of VFG is around 100 nm. The selected area electron diffraction pattern (SAED) corresponding to the VFG is presented in the inset of Fig. 3c, which can be indexed to show that the diffraction rings are the rings of the (002), (100), (004), and (110) planes of polycrystalline graphite. This suggests that as-grown VFG have a typically graphitic crystalline structure. The HRTEM image (Fig. 3d) shows a typical edge of the obtained VFG, with interplanar spacing of 0.34 nm, and the edge of the VFG is approximately 4 to 6 layers of graphene. In order to better investigate the specific surface area of the obtained VFG samples, Brunauer-Emmett-Teller (BET) measurements were performed (Because of the relatively small quantity of VFG grown on the Pt film, as well as the extremely difficult exfoliation of massive and complete VFG from Pt film, VFG grown on Cu foil was used instead to perform the BET measurements due to its suitability for large area preparation of VFG and easy chemical exfoliation). The

obtained specific surface area of VFG is around 430 m^2/g. As the measurement of the accurate specific surface area of VFG-nanocup and VFG-plane is beyond the experimental conditions, the measurement of the VFG loading level on Pt film is another effective method to compare their specific surface area. It is mainly attributed to the vertically standing and non-stacking structure of VFG, which makes it reasonable that higher loading level of VFG means more VFG nanosheets existence, and furthermore, more specific surface area. Based on a number of weight measurements, the loading level of the VFG in VFG-nanocup is estimated to be about 0.0025 mg/cm^2 (estimated: the specific surface area of the VFG-nanocup is 1.08×10^{-3} m^2/cm^2), which more than doubles over that of VFG-plane (0.001 mg/cm^2, the specific surface area of the VFG-plane is 0.43×10^{-3} m^2/cm^2). Therefore, this result clearly demonstrates that the 3D nanocup structure greatly enlarges the surface area for VFG growth than a planar substrate, and the additional high-density VFG nanosheets consequently increase the effective electrode-electrolyte interface for charge storage.

More details about the crystalline quality and graphitic structure of the VFG-plane and VFG-nanocup can be obtained from the Raman spectroscopy data presented in Fig. 4. The Raman spectrum of the samples shows three major bands, i.e., the disorder-induced D band near 1350 cm^{-1}, the G band near 1580 cm^{-1}, attributed to in-plane sp^2 phonon vibrations, and the 2D band near 2700 cm^{-1}, whose position and shape are related to the structure of graphene, especially the layer number.[22-25] The intensity ratio of the D to G bands (I_D/I_G) is related to the degree of disorder and defects in graphene.[26] The I_D/I_G ratios of VFG-plane and VFG-nanocup are 1.49 and 1.50 respectively, indicating that VFG-plane and VFG-nanocup have similar level of structural disorder and crystal defects. The relatively high I_D/I_G value of

PECVD-grown VFG not just comes from the distortion and vacancies in graphitic lattices of VFG formed by plasma bombardment in PECVD growth process, but also is the result of the vertical growth direction of VFG in PECVD, which leads to a high density of open and disordered edges or grain boundary on the top scattering more Raman signal.[25, 27, 28] The intensity ratio of the 2D to G bands (I_{2D}/I_G) can be used to characterize the number and stacking of graphene layers.[22] The I_{2D}/I_G ratios of VFG-plane and VFG-nanocup are 0.73 and 0.75, respectively. This suggests that the as-grown VFG should be few-layer graphene and the average thickness of the VFG varies between 3 and 10 atomic layers.[23] HRTEM was also used to examine the thickness of the as-grown VFG directly. HRTEM images in Fig. 2f and 3d show that the thickness of the VFG is approximately 3 to 6 layers, which confirms that the Raman spectrum gives valid evidence of the thickness of the as-grown VFG. Comparing the Raman results of the two samples, the degree of disorder and the layer number of graphene in VFG-plane and VFG-nanocup are basically the same.

XPS was performed to analyze the chemical composition and valence states of the prepared graphene in VFG-nanocup and VFG-plane. The XPS spectrums of both samples mainly consist of a strong C 1s peak at 284eV and a relatively weak O 1s peak at 533eV,[25, 29-31] as shown in Fig. 5. The atomic concentration for C and O in both samples is estimated to be 98% and 2% respectively, indicating that few oxygen-doped defects or oxygen functional groups exist in VFG samples. This slight contamination is mainly attributed to C–O and C=O formed by physical or chemical adsorption at the surface of VFG nanosheets when exposed to ambient conditions,[32] which has little effect on the electrochemical performance of VFG.

Based on the SEM, TEM, Raman and XPS results, some inferences can be proposed, as follows: (1) Although the morphologies of the substrate surface remarkably varies

between plane and nanocup, the surface morphology and microstructure of as-grown VFG remain similar under the same preparation conditions. This can be attributed to the self-assembly growth mechanism of VFG by PECVD, which is only dependent on the experimental conditions.[32] (2) A large number of vertical graphene walls and exposed edge planes in as-grown VFG can potentially provide not only more area for the electrolyte ions to interact with the electrode surface, but also more accessible electron separation and mobility paths to the current collector, which reasonably lead to the enhancement of supercapacitor performance. (3) It is known that as a support for energy storage, the areal quantity and specific surface area of as-grown VFG are the most critical determinants of the electrochemical properties in supercapacitors.[3] As shown in Fig. 2 and 3, the enlarged surface area of Pt nanocups highly increases the density of as-grown VFG, which consequently achieves a larger specific surface area for energy storage. Thus, the utilization of 3D VFG-nanocup electrodes can enhance the energy-storage performance of supercapacitors by providing a markedly larger surface area for VFG growth than VFG-plane.

To analyze the electrochemical performance of VFG-plane and VFG-nanocup, we performed cyclic voltammetry (CV), galvanostatic charge/discharge (CD), and self-discharge testing in a three-electrode system containing an aqueous electrolyte of 6 M KOH within the potential window from -0.2 to 0.4 V *vs*. a saturated calomel electrode. Fig. 6 shows the CV curves of VFG-plane and VFG-nanocup measured with various voltage scan rates in the range of 2~50 mV/s. It is clear that with increasing voltage scan rate, the area of the CV curves is gradually increased. All the curves maintain an approximately rectangular shape at each scan rate, symmetric in the anodic and cathodic directions, indicating a predominant EDLC characteristic. This means that the double layer formed at the interface is homogeneous and ideally

polarizable in both VFG-plane and VFG-nanocup.[8, 13, 16, 33-36.] In addition, the rectangular shape of all curves displays a deviation in which the delay of the current to reach a horizontal value emerges after the reversal of the voltage sweep, especially at high voltage scan rates, as shown in Fig. 6. This is a typical behavior (distributed capacitance effect) of electrodes based on 3D structured materials.[36, 37] The charge stored in 3D structured materials is distributed, and the Ohmic resistance in the electrolyte along the axial direction of micropores will result in a potential difference.[36, 37] Consequently, the CV curves display a clear deviation in both VFG-plane and VFG-nanocup as a result of the vertically oriented and open-edge structure of as-grown VFG.

Fig. 7a shows the CV curves of the Pt film, VFG-plane and VFG-nanocup at a voltage scan rate of 50 mV/s. The CV curve of Pt film is nearly a straight line with little double-layer capacitance behavior, which may come from the few charge accumulation at the incompletely smooth surface of Pt film. It indicates that the effect of the Pt film (The calculated specific capacitance of Pt film@50 mV/s is ~23 $\mu F/cm^2$ or even lower) is extremely weak on the specific capacitance, and even can be ignored. The CV curve of VFG-nanocup exhibits a markedly enlarged integral area compared with that of VFG-plane, indicating an enhancement of capacitance. Moreover, it can be seen that a more obvious increased slope deviation (distributed capacitance effect) of the current plateau after the reversal of the voltage sweep exists in the CV curve of VFG-nanocup than that of VFG-plane. This may be due to the introduction of the 3D VFG-nanocup hybrid structure, which has a more complicated 3D hybrid structure with a high density of VFG, thereby enhancing the potential difference. Fig. 7b shows the measured specific capacitances of electrodes based on VFG-plane and VFG-nanocup at various voltage scan rates (2~50 mV/s). The VFG-nanocup exhibits

an excellent specific capacitance at all scan rates compared with VFG-plane. In particular, the VFG-nanocup exhibits an ultra-high specific capacitance up to 1052 $\mu F/cm^2$ at the voltage scan rate of 2 mV/s, nearly triple that of VFG-plane (337 $\mu F/cm^2$). These results demonstrate that the utilization of 3D VFG-nanocup is conducive to achieving considerably enhanced capacitance by highly increasing the density of as-grown VFG, and consequently providing more specific surface area for charge storage.

Fig. 7c shows the galvanostatic CD curve of VFG-nanocup at a current density of 0.1 mA/cm^2. Even after many charge/discharge cycles (> 1000 cycles), the curve remains symmetric. Each curve for every charge/discharge duration is close to a triangular shape, without any faradic reaction-induced distortion, confirming a stable charge/discharge process purely ascribed to the EDLC behavior of the electrodes and good charge propagation across the two electrodes.[10, 38] Moreover, no obvious voltage (IR) drops exist at the start of all discharge curves, indicating a relatively low internal resistance.[14, 39] This result suggests that the electrode materials have excellent electrical conductivity, consisting of high electron mobility in the Pt film and VFG, especially the high-quality contact of in situ grown VFG on the Pt film, which can potentially reduce the contact resistance. Based on the discharge curves (the current density of 0.1 mA/cm^2), the energy density of VFG-nanocup can be obtained as 4.88×10^{-4} Wh/m^2, which is nearly three times higher than that of VFG-plane (1.83×10^{-4} Wh/m^2). This improved that energy is mainly attributed to the highly increased specific surface area in VFG-nanocup for charge transmission and storage. Besides, both the VFG-nanocup and VFG-plane possess a high power density around 0.3 W/m^2, indicating a low intrinsic resistance of the electrodes and a fast charge/discharge process between the active material and the electrolyte.

A long cycle life for a supercapacitor is significant for practical applications. The cycle durability of VFG-nanocup was tested by cyclic charge/discharge (CCD) at a current density of 0.1 mA/cm^2, as shown in Fig. 7d. The specific capacitance of VFG-nanocup exhibits a good stability, retaining about 93% of the original capacitance after 3000 cycles. This result suggests that the VFG-nanocup hybrid structured electrode possesses excellent stability, lifetime, and a very high degree of reversibility in repetitive charge/discharge cycling.

To further investigate the electrochemistry of the VFG-plane and VFG-nanocup electrodes, the complex-plane electrochemical impedance spectrum (EIS) was investigated in a three-electrode symmetrical system. Fig. 8 shows the Nyquist plots, Bode phase angle plots coupled with the AC impedance equivalent circuit for the Pt film, VFG-plane and VFG-nanocup samples obtained in 6 M KOH at a DC bias of 0 V over a frequency ranges of 100 kHz to 100 mHz. As shown in Fig. 8a, it is clear that the shape and variation tendencies of both curves are approximately identical. The near-vertical curves indicate a good double-layer capacitance behavior,[40, 41] representative of ion diffusion in the electrode structure.[42] The more vertical the curve is, the more the supercapacitor behaves as an ideal capacitor.[33] The inset of Fig. 8a shows the details of the curves in the high-frequency region. The semicircle at high frequency in the Nyquist plots represents the R_{ct} in the equivalent circuit (see Fig. 8d) which depends on the conductivity at the interface between the active material and the electrolyte, the porous morphology of the electrode material and the thickness of the active material.[43, 44] For both VFG-nanocup and VFG-plane, the semicircle is nearly invisible, suggesting a significantly excellent interfacial charge-transfer behavior in VFG-aqueous electrolyte system. The 45° sloped portion of the Nyquist plots at the end of low-frequency region represents Warburg diffusion stage (W_o), which is a

result of the frequency dependence of ion diffusion in the electrolyte to the electrode interface.[3, 42, 45] The 45° portion of the curve for VFG-nanocup is longer than that for VFG-plane, as shown in the inset of Fig. 8a. This may be associated with the higher density of as-grown VFG in VFG-nanocup than in VFG-plane, which leads to more paths for ion diffusion in a VFG-aqueous electrolyte system.

Fig. 8b shows the Nyquist plots of pure Pt film, VFG-plane, and VFG-nanocup in the high-frequency region. The intercept of the plots with the real impedance in the range of high frequency represents the equivalent series resistance (ESR) of the system, corresponding with the first R_s in the equivalent circuit (see Fig. 8d).[46] It includes the electrolyte resistance, the intrinsic resistance of the active electrode material (VFG), and the contact resistance at the interface of the active material and the current collector (Pt film).[43, 46, 47] Based on the ESR of all samples, the intrinsic resistance and contact resistance of both VFG-nanocup and VFG-plane can be estimated to be around 1.45 Ω, and Pt film around 1.30 Ω. This similar low resistance suggests a good ion response at high-frequency ranges, as well as high-quality contact at the interface of the Pt film and VFG prepared by in situ growth in both VFG-plane and VFG-nanocup. Moreover, the ESR of both VFG-plane and VFG-nanocup remain the same (around 1.45 Ω), suggesting that the enhancement of supercapacitor performance can be attributed to the effect of the 3D VFG-nanocup hybrid structure, which contributes to the higher specific surface for ion transmission and storage in the VFG-aqueous electrolyte system.

Fig. 8c shows the Bode phase angle plots for the Pt film, VFG-plane and VFG-nanocup. the phase angle of Pt film, VFG-nanocup and VFG-plane is 79.69°, 80.2° and 77.84° at 1 Hz, respectively, which is close to that of an ideal capacitor (phase angle is about -90°),[48] suggesting that all samples exhibit a good capacitive

behavior.

Based on these results and discussion, it can be concluded that the 3D VFG-nanocup hybrid structured electrodes possess the following remarkable superiorities for applications in supercapacitors. First, the introduction of the 3D nanocup structure greatly enlarges the surface area for VFG growth, and the additional high-density VFG nanosheets consequently increase the effective electrode-electrolyte interface for charge storage. Second, the morphology of the non-stacked 3D-structured VFG nanosheets optimizes ion diffusion and storage channels, as well as increasing the effective surface area. Finally, the in situ growth of VFG on the Pt film leads to a relatively low contact resistance at the interface of the active material and the current collector.

4. Conclusions

In summary, we have successfully achieved a *one-step* fabrication approach for high-performance supercapacitors using VFG grown in situ on Pt nanocups to form 3D VFG-nanocup hybrid structured electrodes. The VFG-nanocup hybrid structure greatly enlarges the effective surface area of the electrodes and facilitates efficient access of ion diffusion and storage. Moreover, the in situ growth of VFG on the Pt film enables excellent contact quality. The 3D VFG-nanocup hybrid structured electrode exhibits a high specific capacitance up to 1052 $\mu F/cm^2$, and a long cycle life. This 3D VFG-nanocup hybrid structured electrode shows great promise for future utilization in high-performance supercapacitors.

Acknowledgement

The support from the National Natural Science Foundation of China (Grant Nos 51105108), and the Fundamental Research Funds for the Central Universities (Grant No. HIT. NSRIF. 2010113), China, is highly appreciated.

References

1. H. Jiang, P. S. Lee and C. Z. Li, *Energy Environ. Sci.*, 2013, 6, 41–53.
2. X. Zhang, H. T. Zhang, C. Li, K. Wang, X. Z. Sun and Y. W. Ma, *RSC Adv.*, 2014, 4, 45862–45884.
3. J. R. Miller, R. A. Outlaw and B. C. Holloway, *Science*, 2010, 329, 1637–1639.
4. Y. B. Tan and J. M. Lee, *J. Mater. Chem. A*, 2013, 1, 14814–14843.
5. A. Janes, H. Kurig, E. Lust, *Carbon*, 2007, 45, 1226–1233.
6. L. L. Zhang, Y. Gu and X. S. Zhao, *J. Mater. Chem. A*, 2013, 1, 9395–9408.
7. L. Zhao, L. Z. Fan, M. Q. Zhou, H. Guan, S. Y. Qiao, M. Antonietti and M. M. Titirici, *Adv. Mater.*, 2010, 22, 5202–5206.
8. Z. Bo, Z. H. Wen, H. Kim, G. H. Lu, K. H. Yu and J. H. Chen, *Carbon*, 2012, 50, 4379–4387.
9. H. Y. Jung, M. B. Karimi, M. G. Hahm, P. M. Ajayan and Y. J. Jung, *Sci. Rep.*, 2012, 2, 773.
10. J. J. Yoo, K. Balakrishnan, J. S. Huang, V. Meunier, B. G. Sumpter, A. Srivastava, M. Conway, A. L. M. Reddy, J. Yu, R. Vajtai and P. M. Ajayan, *Nano Lett.*, 2011, 11, 1423–1427.
11. Y. Yoon, K. Lee, S. Kwon, S. Seo, H. Yoo, S. Kim, Y. Shin, Y. Park, D. Kim, J. Y. Choi and H. Lee, *ACS Nano*, 2014, 8, 4580–4590.
12. X. H. Cao, Z. Y. Yin and H. Zhang, *Energy Environ. Sci.*, 2014, 7, 1850–1865.
13. M. G. Hahm, R. A. M. Reddy, D. P. Cole, M. Rivera, J. A. Vento, J. Nam, H. Y. Jung, Y. L. Kim, N. T. Narayanan, D. P. Hashim, C. Galande, Y. J. Jung, M. Bundy, S. Karna, P. M. Ajayan and R. Vajtai, *Nano Lett.*, 2012, 12, 5616–5621.
14. Z. Bo, W. G. Zhu, W. Ma, Z. H. Wen, X. R. Shuai, J. H. Chen, J. H. Yan, Z. H. Wang, K. F. Cen and X. L. Feng, *Adv. Mater.*, 2013, 25, 5799–5806.

15. Y. W. Zhu, S. Murali, M. D. Stoller, K. J. Ganesh, W. W. Cai, P. J. Ferreira, A. Pirkle, R. M. Wallace, K. A. Cychosz, M. Thommes, D. Su, E. A. Stach and R. S. Ruoff, *Science*, 2011, 332, 1537–1541.

16. M. D. Stoller, S. J. Park, Y. W. Zhu, J. H. An and R. S. Ruoff, *Nano Lett.*, 2008, 8, 3498–3502.

17. Q. Jiang, H. Y. Tong, D. T. Hsu, K. Okuyama and F. G. Shi, *Thin Solid Films*, 1998, 312, 357–361.

18. R. Yu, H. Song, X. F. Zhang and P. Yang, *J. Am. Chem. Soc.*, 2005, 109, 6940–6943.

19. F. Matino, L. Persano, V. Arima, D. Pisignano, R. I. R. Blyth, R. Cingolani and R. Rinaldi, *Phys. Rev. B*, 2005, 72, 085437.

20. D. Raoufi, A. Kiasatpour, H. R. Fallah, A. Sayid and H. Rozatian, *Appl. Surf. Sci.*, 2007, 253, 9085–9090.

21. N. Eustathopoulos, P. Protsenko, J. P. Garandet and R. Voytovych, *Acta Mater.*, 2010, 58, 6565–6574.

22. Z. H. Ni, H. M. Wang, J. Kasim, H. M. Fan, T. Yu, Y. H. Wu, Y. P. Feng and Z. X. Shen, *Nano lett.*, 2007, 7, 2758–2763.

23. Z. Wang, M. Shoji, K. Baba, T. Ito and H. Ogata, *Carbon*, 2014, 67, 326–335.

24. J. H. Deng, R. T. Zheng, Y. M. Yang, Y. Zhao and G. A. Cheng, *Carbon*, 2012, 50, 4732–4737.

25. C. Y. Yang, H. Bi, D. Y. Wan, F. Q. Huang, X. M. Xie and M. H. Jiang, *J. Mater. Chem. A*, 2013, 1, 770–775.

26. A. C. Ferrari, J. C. Meyer, V. Scardaci, C. Casiraghi, M. Lazzeri, F. Mauri, S. Piscanec, D. Jiang, K. S. Novoselov, S. Roth and A. K. Geim, Phys. *Rev. Lett.*, 2006, 97, 187401–187405.

27. Z. Bo, Y. Yang, J. H. Chen, K. H. Yu, J. H. Yan and K. F. Can, *Nanoscale*, 2013, 5, 5180–5204.

28. M. Cai, R. A. Outlaw, S. M. Butler and J. R. Miller, *Carbon*, 2012, 50, 5481–5488.

29. R. A. Quinlan, M. Z. Cai, R. A. Outlaw, S. M. Butler, J. R. Miller and A. N. Mansour, *Carbon*, 2013, 64, 92–100.

30. C. M. Zhao, X. Wang, S. M. Wang, Y. Y. Wang, Y. X. Zhao and W. T. Zheng, *Int. J. Hydrogen Energy*, 2012, 37, 11846–11852.

31. S. M. Wang, Y. H. Pei, H. Wang, Q. N. Meng, H. W. Tian, X. L. Zheng, W. T. Zheng and Y. C. Liu, *J. Phys. D: Appl. Phys.*, 2010, 43, 455402–455408.

32. L. L. Jiang, T. Z. Yang, F. Liu, J. Dong, Z. H. Yao, C. M. Shen, S. Z. Deng, N. S. Xu, Y. Q. Liu and H. J. Gao, *Adv. Mater.*, 2013, 25, 250–255.

33. C. G. Liu, Z. N. Yu, D. Neff, A. Zhamu and B. Z. Jang, *Nano Lett.*, 2010, 10, 4863–4868.

34. S. Stankovich, D. A. Dikin, G. H. B. Dommett, K. M. Kohlhaas, E. J. Zimney, E. A. Stach, R. D. Piner, S. T. Nguyen and R. S. Ruoff, *Nature*, 2006, 442, 282–286.

35. M. Inagaki, H. Konno and O. Tanaike, *J. Power Sources*, 2010, 195, 7880–7903.

36. T. C. Weng and H. Teng, *J. Electrochem. Soc.*, 2001, 148, 368–373.

37. J. R. Miller, *IEEE Electr. Insul. M.*, 2010, 26, 40–47.

38. J. Yan, T. Wei, B. Shao, Z. J. Fan, W. Z. Qian, M. L. Zhang and F. Wei, *Carbon*, 2010, 48, 487–493.

39. M. F. EL-Kady, V. Strong, S. Dubin, R. B. Kaner, *Science*, 2012, 335, 1326–1330.

40. L. L. Zhang, X. Zhao, M. D. Stoller, Y. W. Zhu, H. X. Ji, S. Murali, Y. P. Wu, S. Perales, B. Clevenger and R. S. Ruoff, *Nano Lett.*, 2012, 12, 1806–1812.

41. Y. Y. Li, Z. S. Li and P. K. Shen, *Adv. Mater.*, 2013, 25, 2474–2480.

42. Y. Wang, Z. Q. Shi, Y. Huang, Y. F. Ma, C. Y. Wang, M. M. Chen and Y. S. Chen, *J. Phys. Chem.* C, 2009, 113, 13103–13107.

43. X. Li, J. P. Rong and B. Q. Wei, *ACS Nano*, 2010, 4, 6039–6049.

44. C. H. Lei, F. Markoulidis and Z. Ashitaka, *Electrochim. Acta*, 2013, 92, 183–187.

45. D. Y. Qu, *J. Power Sources*, 2002, 109, 403–411.

46. C. M. Zhao, W. T. Zheng, X. Wang, H. B. Zhang, X. Q. Cui and H. X. Wang, *Sci. Rep.*, 2013, 3, 2986.

47. D. C. Zhang, X. Zhang, Y. Chen, P. Yu, C. H. Wang and Y. W. Ma, *J. Power Sources*, 2011, 196, 5990–5996.

48. K. Krishnamoorthy, G. K. Veerasubramani, S. Radhakrishnan and S. J. Kim, *Mater. Res. Bull.*, 2014, 50, 499–502.

Figure captions:

Figure 1 Schematic illustrating the fabrication process of the 3D VFG-nanocup hybrid structured electrodes.

Figure 2 (a-d) SEM images, (e) TEM image and (f) HRTEM image of VFG-nanocup. The inset in (c) is the side-view SEM image of the VFG-nanocup.

Figure 3 (a, b) SEM images, (c) TEM image and (d) HRTEM image of VFG-plane. The inset in (b) is the side-view SEM image of the VFG-plane. The inset in (c) is an SAED pattern taken from the corresponding VFG-plane in (c).

Figure 4 Raman spectra of VFG-nanocup and VFG-plane.

Figure 5 XPS spectra for VFG-nanocup and VFG-plane.

Figure 6 CV curves of (a) VFG-nanocup and (b) VFG-plane at the voltage scanning rates of 2, 5, 10, 20 and 50 mV/s, respectively.

Figure 7 (a) CV curves of Pt film, VFG-nanocup and VFG-plane in 6 M KOH at the voltage scan rate of 50 mV/s; (b) specific capacitances of VFG-nanocup and VFG-plane supercapacitors according to the various voltage scan rates in 6 M KOH; (c) charge/discharge curves of VFG-nanocup at a current density of 0.1 mA/cm^2; (d) cyclic stability obtained by performing charge/discharge of the VFG-nanocup supercapacitor at a current density of 0.1 mA/cm^2 over 3000 cycles.

Figure 8 (a) Nyquist plots for VFG-nanocup and VFG-plane, the inset is the magnified portion of the Nyquist plots near the origin; (b) magnified portion of the Nyquist plots for Pt film, VFG-nanocup and VFG-plane near the origin; (c) Bode phase angle plots for Pt film, VFG-nanocup and VFG-plane; (d) AC impedance equivalent circuit.

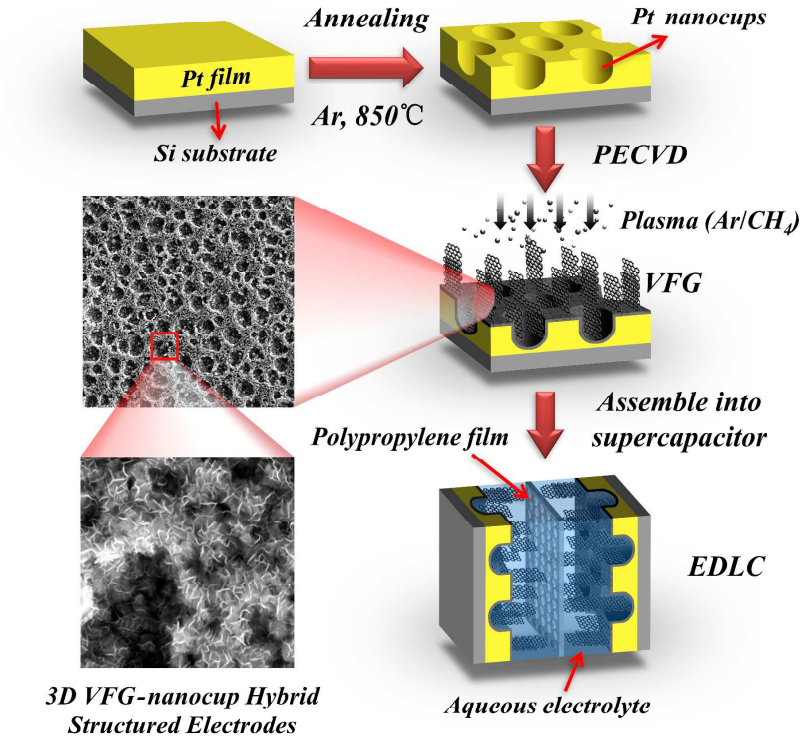

Fig. 1

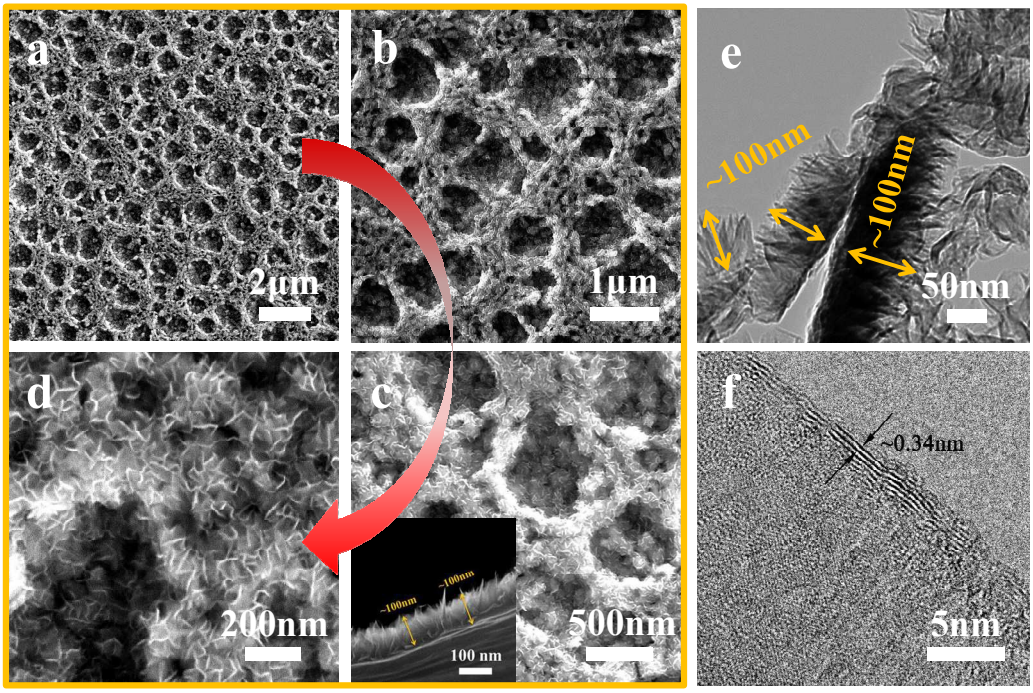

Fig. 2

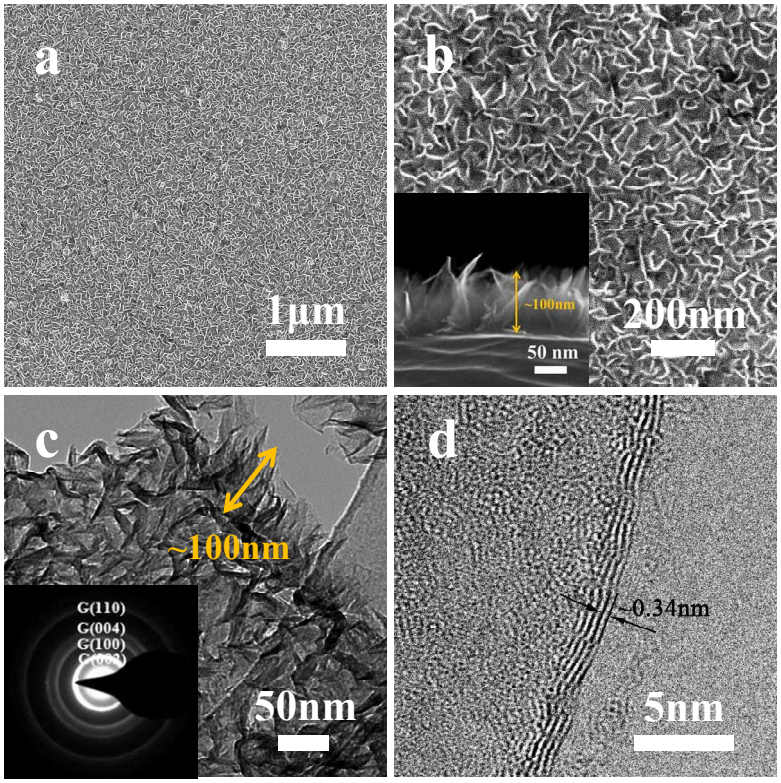

Fig. 3

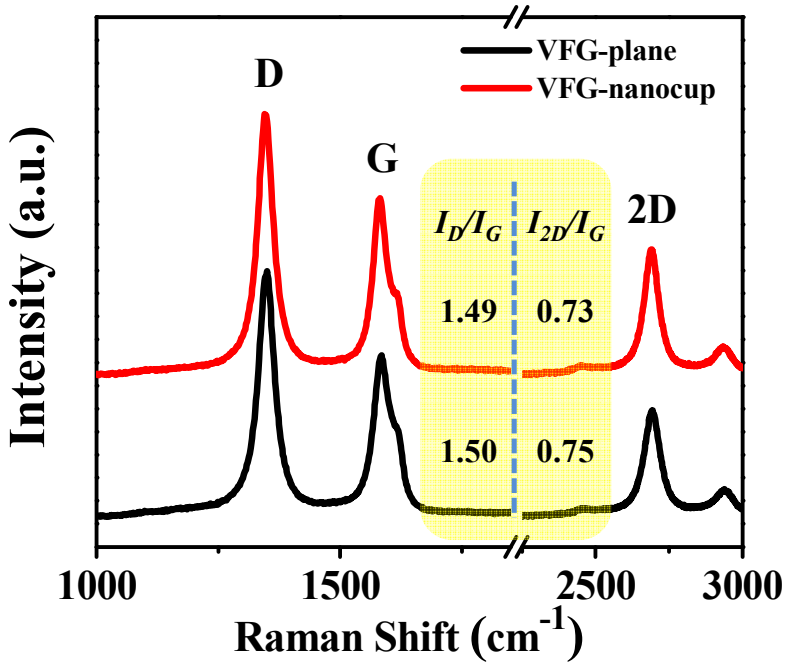

Fig. 4

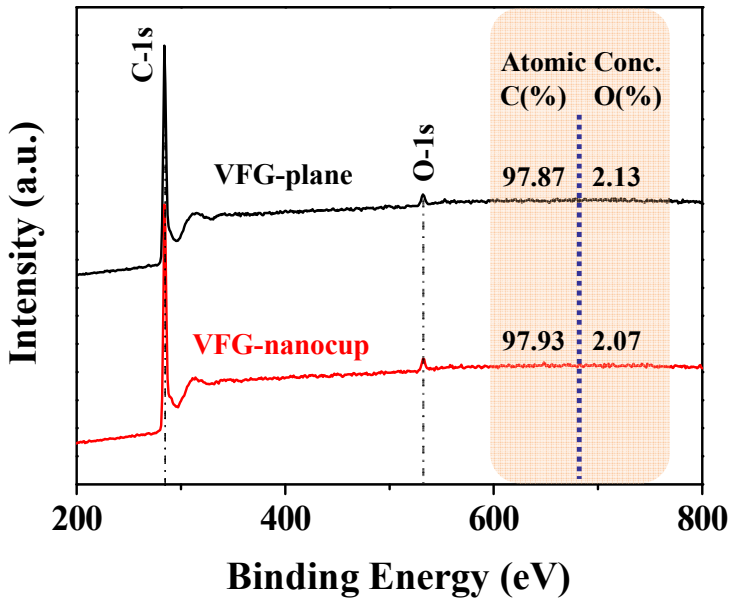

Fig. 5

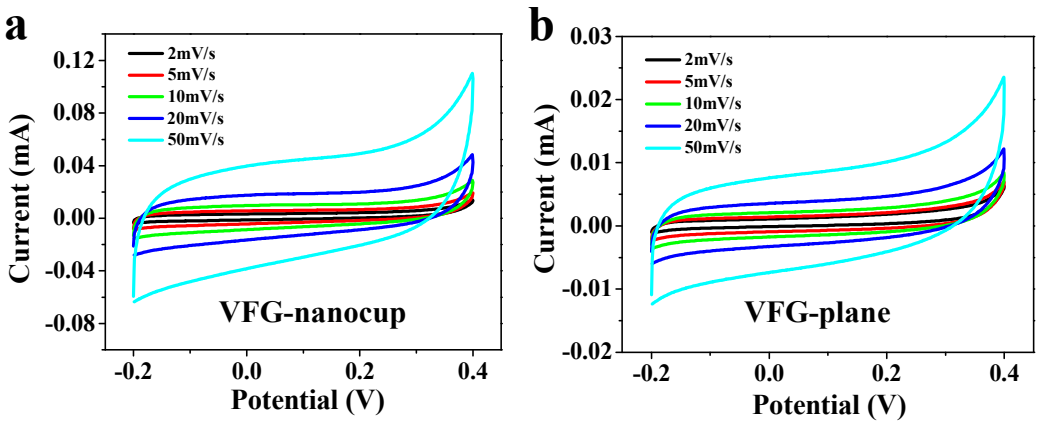

Fig. 6

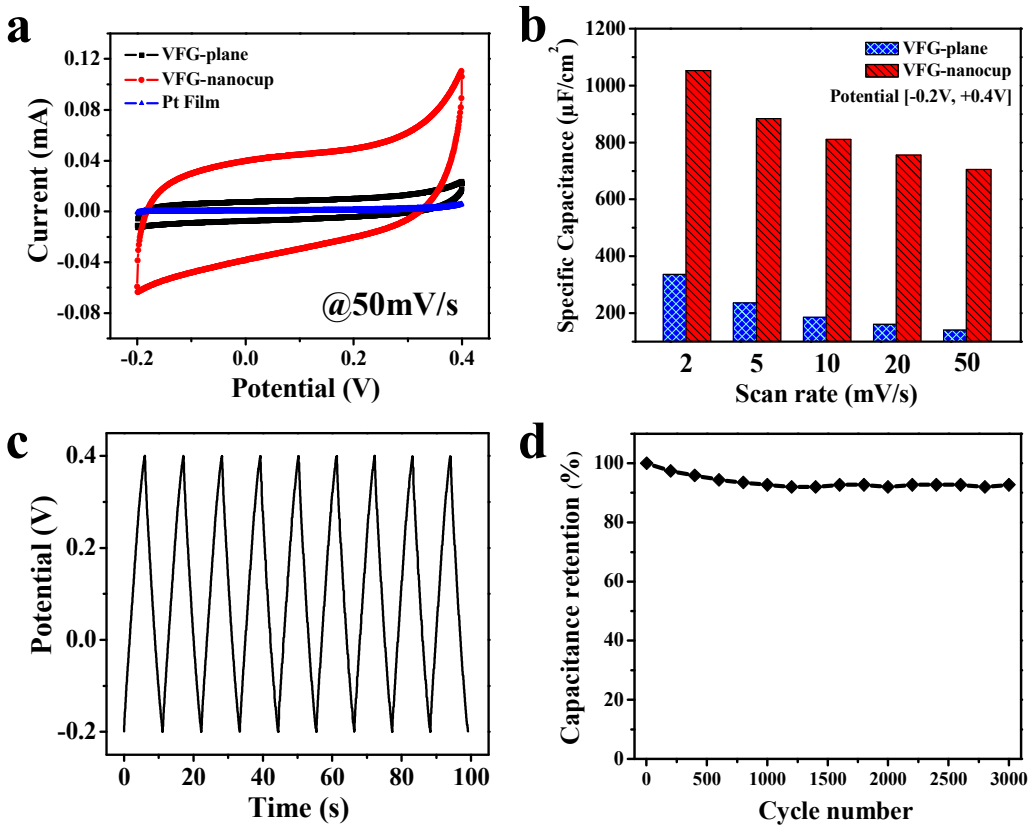

Fig. 7

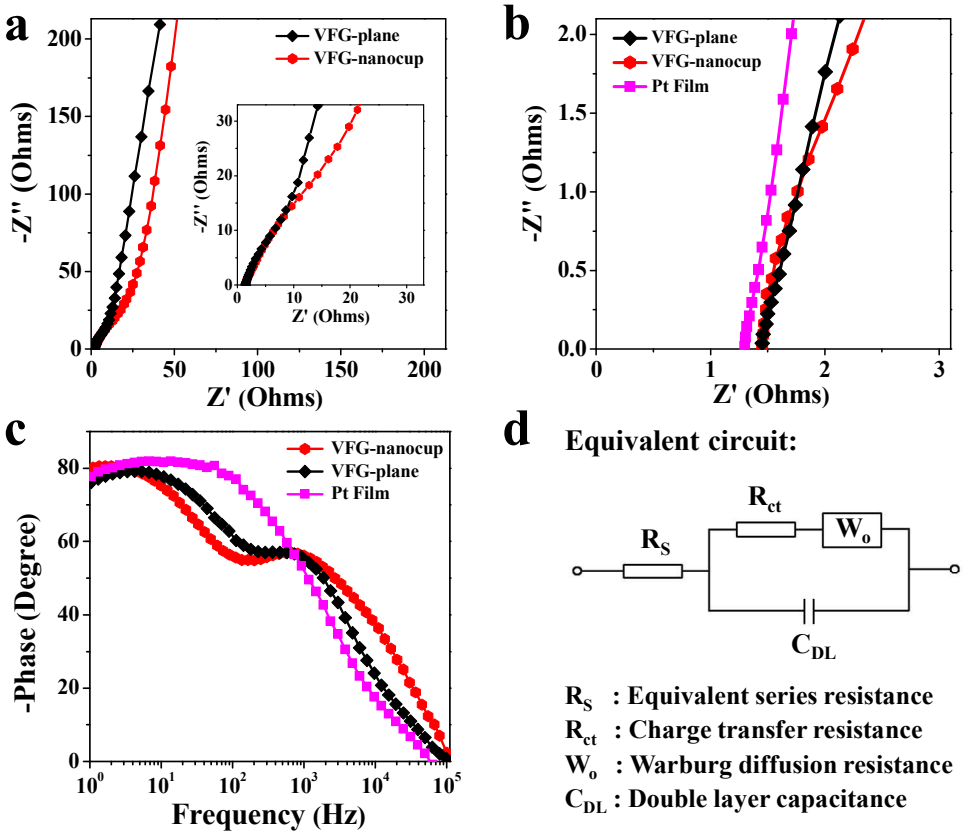

Fig. 8

Graphical Abstract

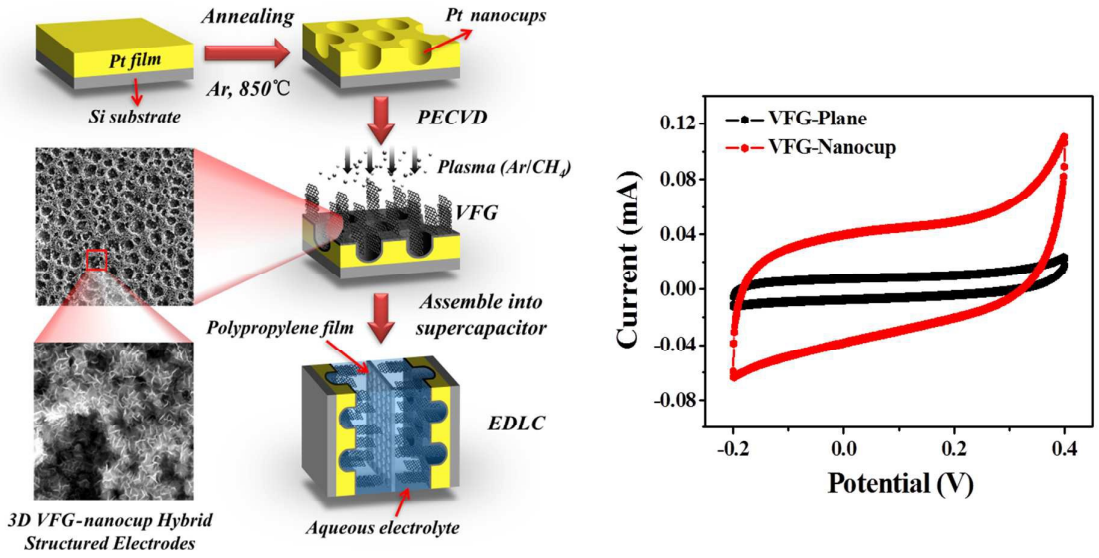

This 3D VFG-nanocup hybrid structured electrode shows great promise for future utilization in high-performance supercapacitors.